Evaluation of existing gas models for gas flow suitable for hydrogen

Review of gas models and flow data

Activity A2.1.2

Task	Activity	Reporting date
2.1	2.1.2	31.01.2024

Title

Evaluation of existing gas models for gas flow suitable of hydrogen

Authors

Hugo Bissig METAS, Eric Starke SICK

Corresponding author

Hugo Bissig

Contributing partners

Rémy Maury CESAME, Hamidou Soumare CESAME, Kurt Rasmussen FORCE TEchnology, Marcel Workamp VSL, Menne Schakel VSL, Alexander Wiener BEV-PTP, Tomas valenta CMI, Mahdi Sadri NEL

Key words

Gas flow, existing models, hydrogen

Notice

This work was funded by the European Union. Views and opinions expressed are however those of the author(s) only and do not necessarily reflect those of the European Union or EURAMET. Neither the European Union nor the granting authority can be held responsible for them.

The contents of this report have been obtained using best scientific practices and have been peer-reviewed prior to release. Nevertheless, the material is provided "as is", without any kind of warranty regarding correctness, completeness, or fitness-for-purpose.

Acknowledgement

The project Met4H2 21GRD05 has received funding from the European Partnership on Metrology, co-financed from the European Union's Horizon Europe Research and Innovation Programme and by the Participating States.

DOI	License	Copyright
n/a	This work is licensed under CC BY 4.0. To view a copy of this license, visit https://creativecommons.org/licenses/by/4.0/	n/a

Feedback

The consortium welcomes feedback. Please send your comments, suggestions or other feedback to the project coordinator, dr. Adriaan van der Veen (VSL), avdveen@vsl.nl.

Summary

A review of the different gas flow meter technologies using various gases is given based on a literature study. Some of the gas meter technologies have been measured with hydrogen as well. For some gas meter technologies predictive models for hydrogen exist and are described in this report.

- Critical flow venturi nozzles have been tested with various gases, where air, nitrogen and hydrogen showed similar behavior for the relative deviations in the same Reynolds number range. An extrapolation model has been presented, but the experimental validation has only been performed with natural gas. Tests with hydrogen are planned in the project MetHyInfra [13].
- Turbine meters have been investigated with blends up to 30 % of hydrogen in natural gas. A predictive model for meter deviation with hydrogen exists, but is has not yet been validated with hydrogen measurements.
- For the rotary meter a predictive model also exists, but measurements have only been performed with natural gas so far. Measurements with hydrogen are still missing.
- Differential pressure meters have only been tested with natural gas. Measurements with hydrogen are still missing.
- Ultrasonic meters have been investigated with blends up to 30 % of hydrogen in natural gas. Measurements with hydrogen are still missing.
- Coriolis flow meters have been investigated with natural gas. Measurements with hydrogen are still missing to validate the CFM model.
- Thermal gas flow meters have been tested with various gases including hydrogen, but the predictive models do not match the experimental results with the necessary accuracy.

Extensive experimental validation of the existing models for the different gas meter technologies are still missing. Therefore, the assessment whether models for air or natural gas can correctly model hydrogen flow is not possible at this stage due to lack of experimental data. Limitations of the models and expected uncertainties need a wide range of datasets to estimate this.

Contents

1 Introduction

The aim of this activity is to evaluate existing models for gas flow suitable for hydrogen. This evaluation shall assess whether models for air or natural gas can correctly model hydrogen flow for different applications and flow conditions and the likely limitations and uncertainties.

A review of the different gas flow meter technologies using various gases is given based on a literature study. Some of the gas meter technologies have been measured with hydrogen as well. For some gas meter technologies predictive models for hydrogen exist and are described in this report.

2 Existing models for gas flow

2.1 Critical flow Venturi Nozzles (CFVN)

2.1.1 Model for CFVN for laminar boundary layers

The critical flow Venturi Nozzles (CFVNs) have proven to be widely used as secondary standards for measuring gas flow rates, where the gas flow rate q_m through the nozzle is defined as [1]

$q_m = C_d \, q_{m,id}$

where C_d is the discharge coefficient and $q_{m,id}$ is the ideal gas flow rate.

The ideal mass flow rate is calculated assuming the one-dimensional isentropic flow of ideal gas [1]:

$$q_{m,id} = \frac{A \, C^* p_0}{\sqrt{R \, T_0 / M}}$$

where A is the cross-section at the nozzle throat calculated using the throat diameter, C^* is the critical flow function, R is the gas constant, M is the molar mass of the gas and p_0 and T_0 are the stagnation pressure and temperature, respectively.

The calculation methodology described in the ISO 9300 assumes that the discharge coefficient depends only on the geometry of the nozzle and the Reynolds number using the dynamic viscosity of the gas at stagnation inlet conditions [2]. However, several models have shown that the discharge coefficient also depends on the thermodynamic properties of the gases.

The discharge coefficient of a sonic nozzle is the product of two almost independent effects [3]:

- viscous effects in the boundary layer $c_{d,visc}$
- multi-dimensional feature of the inviscid core flow displacement effect of the boundary layer $c_{d,inv}$

The discharge coefficient can be expressed by

$$C_d = a \left(1 - \frac{b}{\sqrt{R_e}} + \frac{b^2}{4 \, R_e}\right)$$

where a is the $c_{d,inv}$ being a function of the isentropic exponent and the curvature of nozzle contour at the throat according to Kliegel and Levine [4].

b is a function of the throat curvature and the factor G [5,6,7]. The factor G represents the dependence of the mass flow defect on the velocity and density distribution within the boundary layer and is a function of the isentropic exponent κ, the Prandtl number Pr and the temperature difference between the gas and the nozzle body at the nozzle wall [6,7].

Three different application approaches of the model were investigated by reference [8], where two nozzles were calibrated with six different gases (dry air, argon, helium, hydrogen, nitrogen, nitrous oxide):

- Approach A: coefficients a and b are independent of gas type. Coefficients a and b were obtained by fitting nitrogen data and are also used for other gases.
- Approach B: coefficients a and b are based on $G(\kappa_{N2},Pr_{N2})$. Values of d_{th} and R_C are calculated for nitrogen data and are then used to calculate the coefficients a and b for other gases based on $G(\kappa_{othGas},Pr_{othGas})$. Assumption $Pr = 1$.
- Approach C: same as approach B, but with the actual value of Pr.

In this report, only the deviations of the different approaches by taking nitrogen as reference gas are shown to estimate how consistently the nitrogen calibration result can be applied to other gases. Extensive results can be found in [8].

The deviation ε is defined as

$$\varepsilon = \frac{C_d^{(model)}}{C_d} - 1$$

where C_d is determined upon the experimental data for a particular gas and considering d_{th} for to the selected model. $C_d^{(model)}$ represents the value of the discharge coefficient determined by the selected modelling approach for a specific gas.

"The use of approach C is recommended. The results show that CFVNs used with hydrogen in the tested range of Reynolds numbers in the laminar boundary layer regime can potentially be calibrated with alternative gases. The first choice would probably be air or nitrogen, whose values of discharge coefficients match those of hydrogen quite well. By ensuring a comparable range of Reynolds numbers in the air or nitrogen calibration with that corresponding to hydrogen flow, the calibration results can be directly applied to hydrogen as well, without having to consider additional corrections." (see Figure 1, Figure 2, Figure 3) [8].

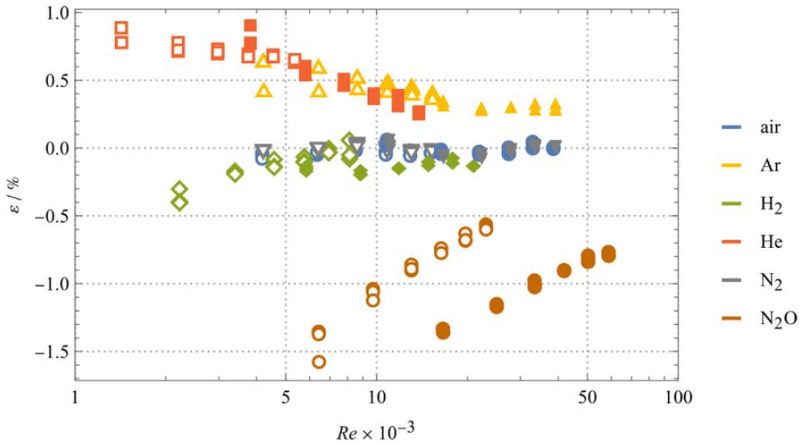

Figure 1: Relative deviations for the approach A for both nozzles (nozzle 1 – hollow markers, nozzle 2 – filled markers); estimated expanded uncertainties of presented data equal 0.17 %. Figure from [8].

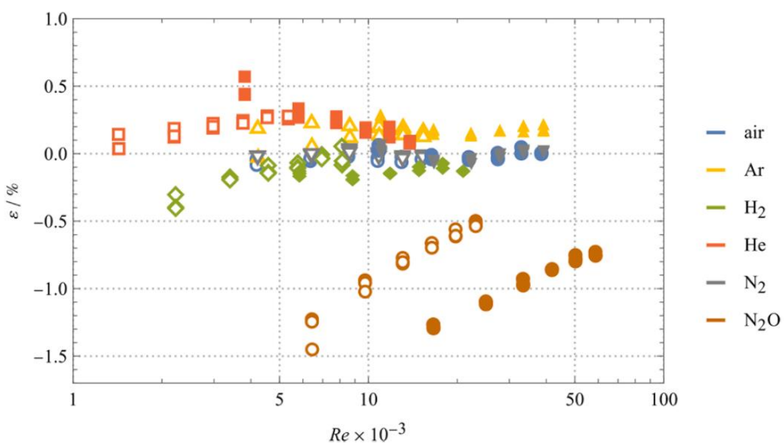

Figure 2: Relative deviations for the approach B for both nozzles (nozzle 1 – hollow markers, nozzle 2 – filled markers); estimated expanded uncertainties of presented data equal 0.17 %. Figure from [8].

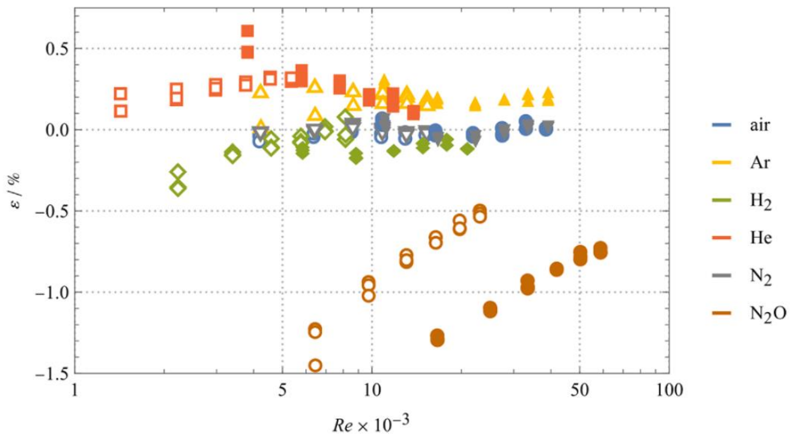

Figure 3: Relative deviations for the approach C for both nozzles (nozzle 1 – hollow markers, nozzle 2 – filled markers); estimated expanded uncertainties of presented data equal 0.17 %. Figure from [8].

2.1.2 Model for CFVN for laminar to turbulent boundary layers - extrapolation model

The functionality for the discharge coefficient C_d versus Reynolds number was successfully introduced to cover the operating of critical nozzles with laminar as well as turbulent boundary layers using only three parameters [9]. The data for atmospheric air usually cover not a wide range of Reynolds numbers. Therefore, investigations have been performed to reduce the number of free parameters to one in order to extrapolate the functionality for the laminar regime to the turbulent regime [10,11]. The dependency of the discharge coefficient on the Reynolds number is different for the laminar and the turbulent boundary layers (BL):

$$C_{d,lam} = a - b_{lam}\, Re^{-0.5}\ for\ laminar\ BL$$

$$C_{d,turb} = a - b_{turb}\, Re^{-0.139}\ for\ turbulent\ BL$$

For the parameters a and b_{lam} are solved theoretically by Kliegel [4] and Geropp [6,7]

To reduce the number of free parameters, the fact was used that the theoretical approaches for parameters a and b_{lam} are both based on the curvature radius. The assumption is made that the virtual curvature radius $R_{C,virt}$ is the same for both parameters. Thus, the following relationship between b_{lam} and b_{turb} was found, valid for hydraulic smooth surfaces and no significant roughness in the nozzles [10,11]:

$$b_{turb} = 0.003654\, b_{lam}^{1.736}$$

The transition function of the discharge coefficient for the whole range of the Reynolds numbers is defined as:

$$C_d = s_{lam} \cdot C_{d,lam} + s_{turb} \cdot C_{d,turb}$$

with

$$s_{lam} = 0.5 \left\{1 - tanh\left[k_u \, log\left(\frac{Re}{Re_{tr}}\right)\right]\right\}$$

$$s_{turb} = 1 - s_{lam}$$

where s_{lam} and s_{turb} are weighing terms, Re_{tr} defines the middle point of the transition and k_u defines the sharpness of the transition.

Based on experience, the parameters are set to k_u = 5.5 and Re_{tr} = $1.25 \cdot 10^6$. These assumptions allow to have the functionality for the discharge coefficient from low to high Reynolds numbers with one free parameter b_{lam}.

Data of 33 nozzles with a minimal throat diameter of 3.8 mm have been chosen to validate the transition function of the discharge coefficient. The discharge coefficients of two nozzles are shown in Figure 4. For the determination of the b_{lam}, only the values of the discharge coefficients measured at Reynolds number below $Re = 10^5$ were used (Figure 4, dark blue circles).

The procedure for the determination of the expectation value $E(C_{d,extrapol})$ is described in detail in [11]. In Figure 4, the measured discharge coefficients with the measurement uncertainties as well as the $E(C_d)$ of the measurements with the 95%-confidence limits for air and natural gas at higher Re are shown.

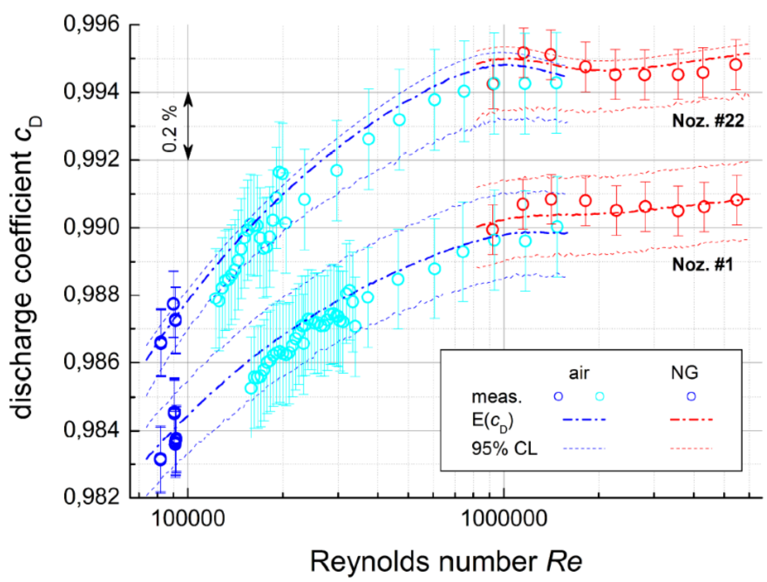

Figure 4: Examplary data of two nozzles with the designed throat curvature radii $R_{C,design}$ = 1 (#1) and $R_{C,design}$ = 2 (#22) [11].

The results show high consistency and the validation of the approach can be shown by the calculation of the difference between the measured discharge coefficient $C_{d,meas}$ and the extrapolated $C_{d,extrapol}$, defined as:

$$\Delta_{C_d} = C_{d,meas} - C_{d,extrapol}$$

In Figure 5, the difference Δ_{Cd} is shown as a function of the Reynolds number for air, natural gas and nitrogen. Most of the data are within ± 0.2 % (for 29 of 33 nozzles). This agreement is independent to the design curvature radius as well as the resulting virtual curvature radius and covers a wide range of nozzles shapes (details in [11]).

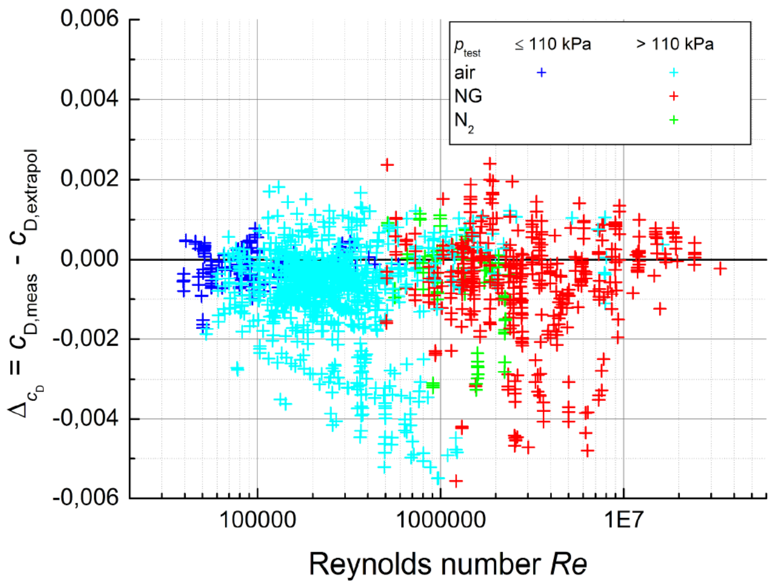

Figure 5: Difference D_{Cd} of the measured discharge coefficients $C_{d,meas}$ to the extrapolated $C_{d,extrapol}$ in dependency on the Reynolds number [11].

Further results can also be found in the reference [12], which confirm this approach for the extrapolation to higher Reynolds numbers.

2.1.3 Model for CFVN for turbulent boundary layers for hydrogen

Investigations of the behavior of nozzles at higher flow rates is planned within the MetHyInfra project, where measurements with toroidal and cylindrical nozzles of different roughness with inert gases (air, nitrogen, helium) will be carried out [13]. These nozzles will also be tested with hydrogen to test the applicability of the extrapolation approach to higher Reynolds numbers.

2.2 Turbine meters (TM)

2.2.1 Model PTB

The fact that the meter deviation of turbine meters is mainly depending on Reynolds number if the momentum ρQ^2 of the flow, where ρ is the density and Q is the flow rate, is strong enough to overrule the friction of the bearings is well known. This is the case for higher flow rates, but at lower flow rates the friction of the bearings gets more important.

The PTB turbine meter model describes the deviation of a turbine gasmeter e_{TM} as the sum of three contributions [14]. For normal operation flow forces are dominant, resulting in a contribution e_{Re}. At low speeds the contribution e_b from the bearing friction becomes important. For high flow velocities there is a contribution e_p due to the expansion of the gas flow between the pressure reference point and the temperature measurement downstream of the meter.

$$e_{TM} = e_{Re} + e_b + e_p$$

with

- $e_{Re} = \sum_{j=0}^{n} a_j [log(Re/10^6)]^j$, flow force contribution with a_j being coefficients that are determined by a least-squares approximation. In practice, n ≤ 4.
- $e_b = \frac{b_0}{\rho Q^2} + \frac{b_1}{\rho Q}$, bearing friction contribution, where b0 and b1 are empirical coefficients determined in so-called spin down test and step response test [15]. The spin down test can be done at PTB under nearly vacuum condition in order to neglect the impact of fluid friction on the wheel. The step response test is applying sudden flow rate changes by means of switching critical nozzles at PTB [16].
- $e_p = c_p Q^2 \frac{\rho}{p}$, high flow velocity contribution, where c_p is an empirical coefficient dependent on the gas composition via the isentropic expansion factor κ.

An example of the application of the turbine meter model is given in reference [14]. The observed deviation e_{TM} of each individual data point is corrected for the influence of the bearing friction e_b and the the high-speed Mach effect e_p, where the coefficients b_0, b_1 and c_p are determined for the corresponding turbine meter. The resulting deviation e_{Re} is plotted as a function of the Reynolds number as shown in Figure 6 and Figure 7.

Most data points agree within their uncertainty with the fit (red line) of the weighted averages of the piston prover calibrations. The data of the atmospheric air calibrations connect to the visual extrapolation of both the red-line and black-line fits of e_{Re}.

The turbine meter model is an adequate method to connect the calibration data obtained with natural gas at different pressures on one side and the calibration data with atmospheric air at the other.

The deviation e_{Re} can then be approximated by an appropriate function of Reynolds number by fitting $e_{Re} = \sum_{j=0}^{n} a_j [log(Re/10^6)]^j$ with n ≤ 4 for the best least-squares fit.

This appropriate function and the parametrized parts e_b and e_p allow to transfer the original calibration to any other gas as long as the Reynolds number stay inside the Reynolds range of the calibration data base.

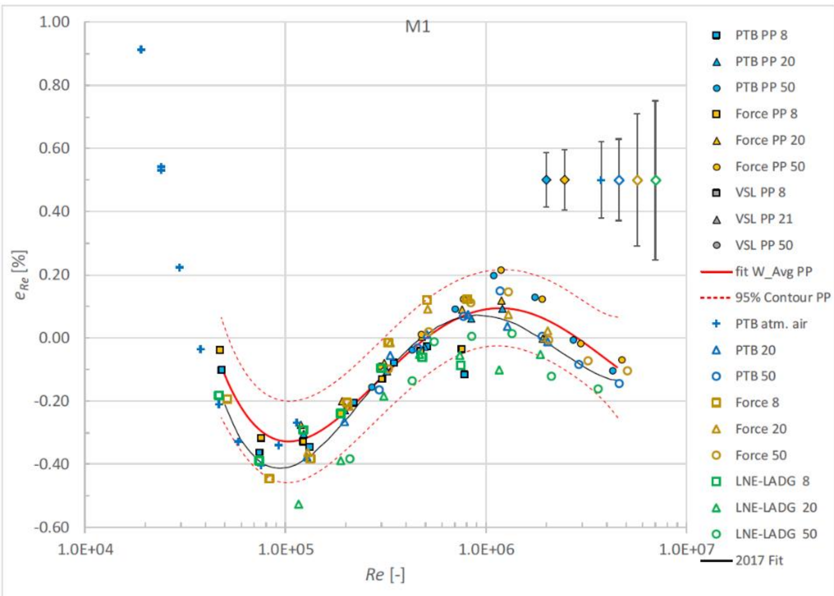

Figure 6: Calibration results of the DN100 turbine gas meter M1. The meter deviation e Re *[%] is plotted versus the Reynolds number* Re *[-] on a logarithmic scale. The solid markers represent the results obtained with the piston provers. The red solid line is the least-squares fit of these results and the dashed lines represent the 95% uncertainty contours. The open markers are the result from the previous intercomparison [17]. The black solid line is the fit of these intercomparison data. The crosses (+) are the calibrations with atmospheric air, which are excluded from the fits. For reference the associated expanded uncertainties are indicated in the upper-right corner. (Figure 2 of Reference [14] in Cal Lab)*

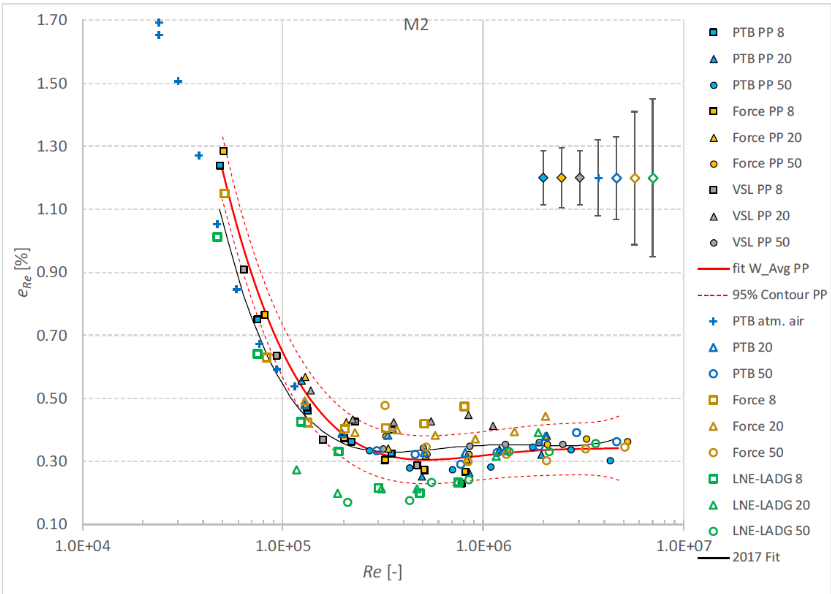

Figure 7: Calibration results of the DN100 turbine gas meter M2. The meter deviation e Re *[%] is plotted versus the Reynolds number* Re *[-] on a logarithmic scale. The solid markers represent the results obtained with the piston provers. The red solid line is the least-squares fit of these results and the dashed lines represent the 95% uncertainty contours. The open markers are the result from the previous intercomparison [17]. The black solid line is the fit of these intercomparison data. The crosses (+) are the calibrations with atmospheric air, which are excluded from the fits. For reference the associated expanded uncertainties are indicated in the upper-right corner. (Figure 2 of Reference [14] in Cal Lab)*

2.2.2 Predictions for meter deviation with hydrogen

An example of the transfer of the original calibration with air to hydrogen is shown in reference [16]. If a turbine meter shall be calibrated for application in hydrogen at 9 bar(a), the similar Reynolds number can be achieved with air at 1 bar with only 26 % higher flow rates due to the other norm density and viscosity of hydrogen compared to air. The part e_{Re} can be considered similar, but the part e_b is significantly different resulting in different e_{TM} curves as shown in Figure 8 by the difference of the two meter curves Δe_{TM}.

For most of the turbine meters with size larger than or equal to DN100, the application in hydrogen at 9 bar(a) and higher will be possible for a turn down ratio of 1:10 or better [16].

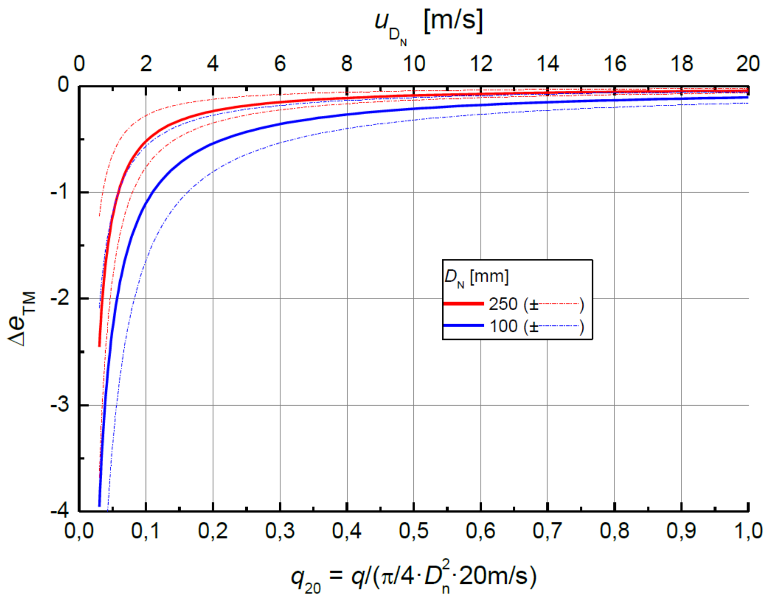

Figure 8: Predicted difference of meter deviations of TMs with DN = 100 mm and DN = 250 mm for usage in Hydrogen@9bar(a) when calibrated with air@1bar applying same Reynolds numbers for a certain flow rate [16].

2.2.3 Results of turbine meter with various gases

Turbine meter have been calibrated with various gases such as nitrogen, methane, natural gas with hydrogen blends up to 30 % and are reported in a conference paper [18]. Repeatability is calculated as twice the standard deviation of the mean value of three consecutive measurement points and results in repeatability values of the order of 0.2 % for all gas mixtures (nitrogen, methane, natural gas with blends of hydrogen from 5 % to 30 % and blends of carbon dioxide) at pressures of 16 bar(a) and 32 bar(a).

Moreover, the meter deviation shows no gas dependence as a function of the Reynolds number, as shown in Figure 9.

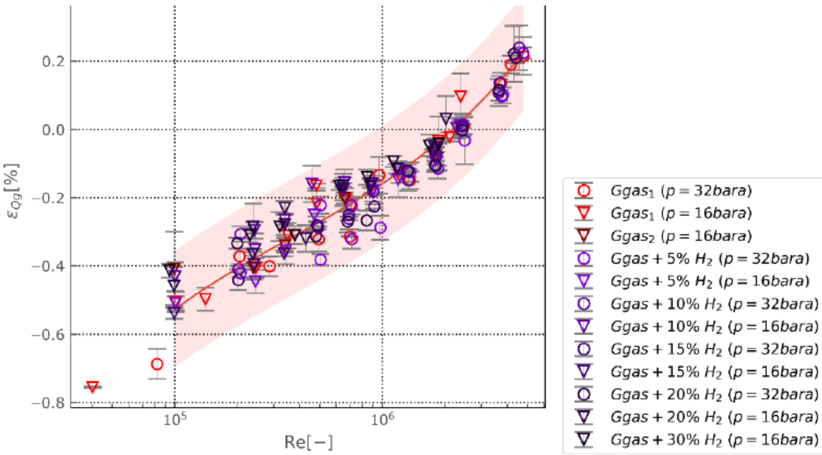

Figure 9: Turbine meter deviation as a function of the Reynolds number. No gas dependence [18].

The flow-weighted mean error (FWME) of three new turbine meters have been calculated according to ISO 17089 [19]. The calculation has been applied to measurements with different gases and the results show no gas dependence as shown in Figure 10.

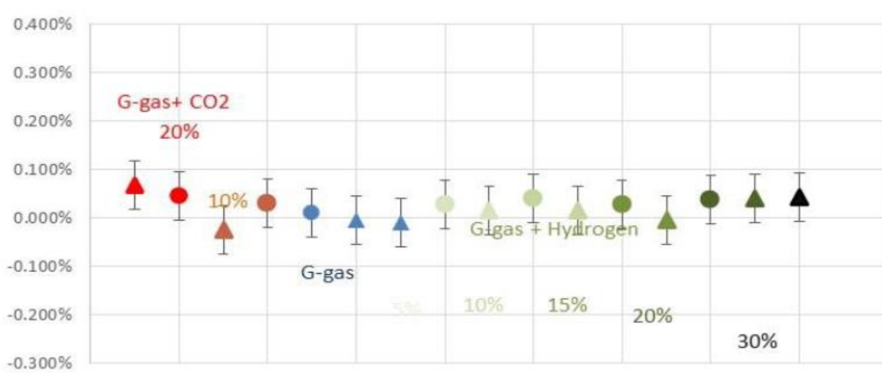

Figure 10: The FWME results of one new turbine meter for various gases (where G-gas is Groningen-gas). No systematic gas composition effect is observed [18].

2.3 Rotary meters (RM)

2.3.1 Model PTB

The meter deviation of rotary meters has a similar background as turbine meters [16]. The characteristics of bearings in rotary meters are very close to that of turbine meters and the resulting torque is linear to the indicated flow rate [15]. Other contributions on the model are the torque caused by the pressure difference across the piston and the drag of the gap flow between the piston and the walls.

All these contributions are developed in reference [16] and the meter deviation e is expressed as

$$e_{RM} = \alpha_{Re}\left[1 + \hat{C}_B \frac{(a + q_i)}{\mu\, q_i}\right] + O_{just}$$

with

$$\alpha_{Re} = \frac{C_{gap,2}\, C_{\tau W}\, C_{\tau,1}}{\left(C_{just} + C_{gap,1}\right)\left(C_{\Delta p} + C_{\tau W} C_{\tau,2}\right)}$$

The parameters α_{Re}, $C_{gap,2}$ and $C_{\tau,2}$ are strongly Reynolds number dependent.

The gap flow between the piston and the wall depends on the viscosity of the laminar or turbulent state of the boundary layer. Therefore, a model for the viscosity has to be defined. For the laminar case it is the molecular viscosity $\mu_{mol.}$, whereas for the turbulent case the so-called eddy viscosity $\mu_{eddy\ visc.}$ is applied.

$$\mu_{mol.} = \frac{4\,\rho\, q_i}{\pi\, D\, Re}$$

$\mu_{eddy\ visc.} = C_{turb}\, \rho\, q_i$ with $C_{turb} = \frac{4\,\rho\, q_i}{\pi\, D\, Re_{tr}}$, where Re_{tr} is the transitional Reynolds number.

To keep the model of the viscosity simple

$$\mu = \begin{cases} \mu_{mol.}\ if\ Re < Re_{tr} \\ \mu_{eddy\ visc.}\ otherwise \end{cases}$$

An example for one rotary meter measurements with atmospheric air, air up to 16 bar and natural gas at 17 bar and 50 bar is described in reference [16]. The meter deviation is shown in Figure 11.

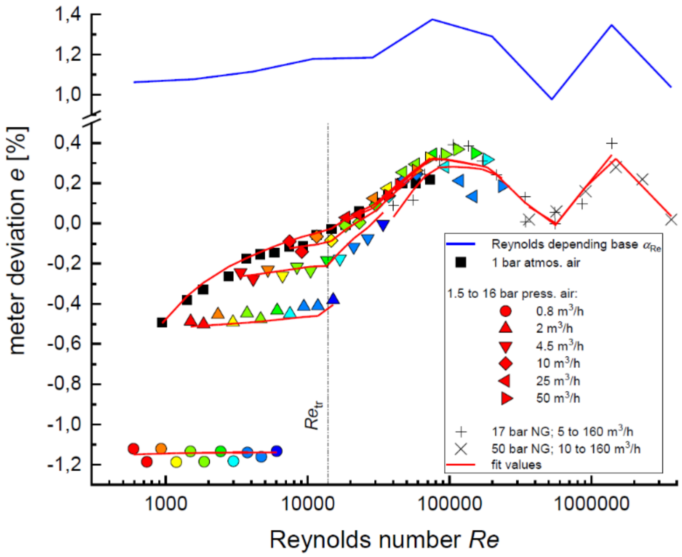

Figure 11: Meter deviations e of a rotary meter for various flow rates, pressures and fluids together with the Reynolds number depending base curve a_{Re} and the fit curve according to the model (red lines) [16].

2.3.2 Predictions for meter deviation with hydrogen

This model can be used to perform the calibration of the rotary meter with atmospheric air and then to calculate the expectation for hydrogen at 9 bar(a) with the parametrization of the meter [16]. The expected meter deviation is shown in Figure 12.

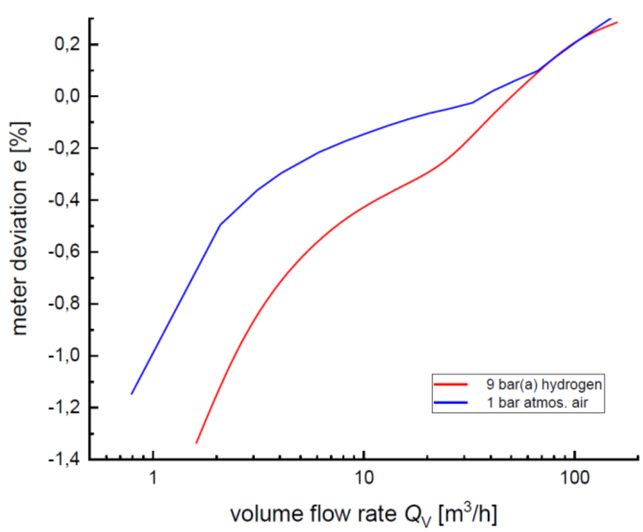

Figure 12: Meter deviation for atmospheric air and the calculated expectation for hydrogen at 9 bar(a) [16].

A high-quality rotary meter with turn down ratio of 1:160 with air is expected to have a turn down ratio of 1:80 with hydrogen.

2.4 Differential Pressure meters (DP) / Orifice meters

Differential pressure meters like orifices designed according to the ISO 5167 [20] have from their physical principle a clear pure dependency on Reynolds number except a correction by means of the expansion number ε for compressible fluids. Therefore, the ISO5167 does not distinguish between different fluids but is valid for wide range of incompressible as well as compressible fluids and is implicitly including also pure hydrogen or blend of natural gas with hydrogen [16].

The discharge coefficient c_D is defined as [20]:

$$c_D = \frac{q_m\sqrt{1-\beta^4}}{\varepsilon\frac{\pi}{4}d^2\sqrt{2\rho_1\Delta p}}$$

Measurements have been performed with water, atmospheric air and natural gas at 17 bar and the measured discharge coefficients as well as the calculated discharge coefficients of the orifice meter are shown in Figure 13 [16].

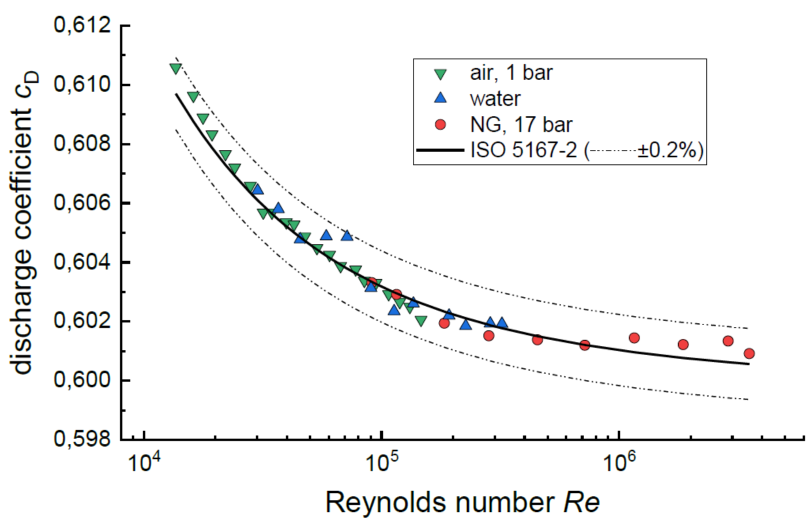

Figure 13: Calibration results of an orifice meter with nominal pipe size of DN 150 in comparison with the reference curve of ISO 5167-2 [16].

2.5 Ultrasonic meters

Ultrasonic flowmeters (USM) for precise gas flow measurement operate according to the transit-time difference method. As for the most flow meter technologies, larger differences in fluid properties requires design adaptations to ensure accurate measurements. In the case of USM, the very high speed of sound and low density of hydrogen compared to natural gas or methane leads to functional differences. To provide a fiscal USM for hydrogen there are a few important design modifications that are needed [21]:

- Standard deviation of the measurement data.
- Measurement value sensitivity to side effects (temperature, pressure and variation in gas composition…) due to the acoustic effects.
- Flow effects on the uncertainty ("installation effects").

The standard deviation of the measurement data,

$$\sigma(Q) \sim \sigma(\Delta t) \cdot c^2$$

is dominated at high flow rates by the turbulence of the flow while at lower flow rates the scattering is dominated by the standard deviation of the transit-time difference measurement Δt. As the speed of sound for hydrogen is three times higher than for natural gas, the standard deviation of the transit-time difference measurement would have to be reduced by a factor nine to maintain the level of $\sigma(Q)$. The increase of the working frequency in the range from 500 kHz to 3 MHz for various meter sizes is expected to reduce the $\sigma(\Delta t)$ for hydrogen applications. Additionally, for sound coupling and decoupling in hydrogen, other transducer concepts than in natural gas have to be used due to the low density.
Acoustic effects, like early and late reflections or transducer ringing, are one reason for sensitivity to side effects. The shape of the sonic beam ("acoustic directivity") has to be adjusted to ensure the necessary beamwidth at the higher speed of sound for hydrogen to reduce effects of wall reflections. This requires adjustments to the ultrasonic transducers for the higher speed of sound range.

For typical designs of USM, the installation effects for natural gas, hydrogen or hydrogen blends should not differ from each other much. Some effects could be expected or fluid mechanical more complex setups like flow conditioners. Ongoing research projects are investigating this [22,23].
With the design adaptations a fiscal hydrogen USM shows advantages in terms of high turn down (>1:100), low pressure drop and a large range of line sizes. Furthermore, USMs offer maximum flow velocities 2 - 3 times higher than in natural gas [21] which enables energy equivalent transport capacity for hydrogen pipeline transport.

Measurements with natural gas, hydrogen blends and carbon dioxide blends have been performed with ultrasonic meters designed for natural gas [18]. The ultrasonic gas meters show drift behaviour that differs from meter-to-meter depending on path configuration, settings and correction algorithms. The flow-weighted mean error (FWME) of ultrasonic gas meters have been calculated according to ISO 17089 [19] and are shown in Figure 14 and Figure 15.

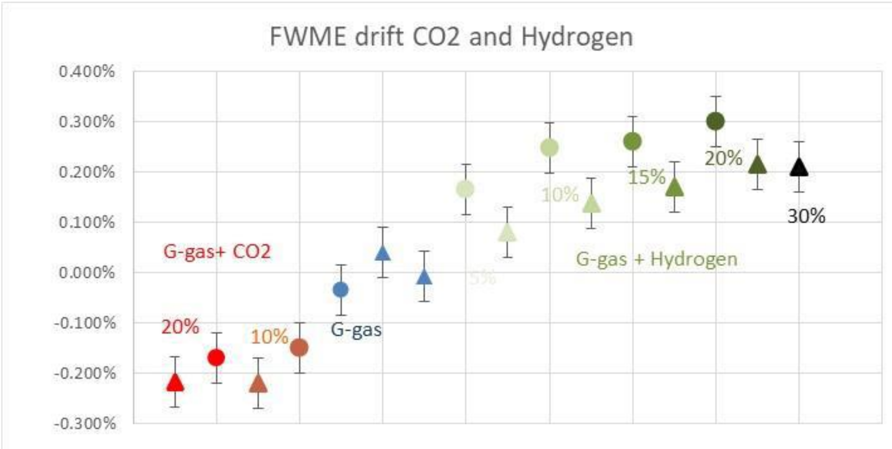

Figure 14: USM designed for natural gas (Example manufacturer A). The FWME results for various gases [18].

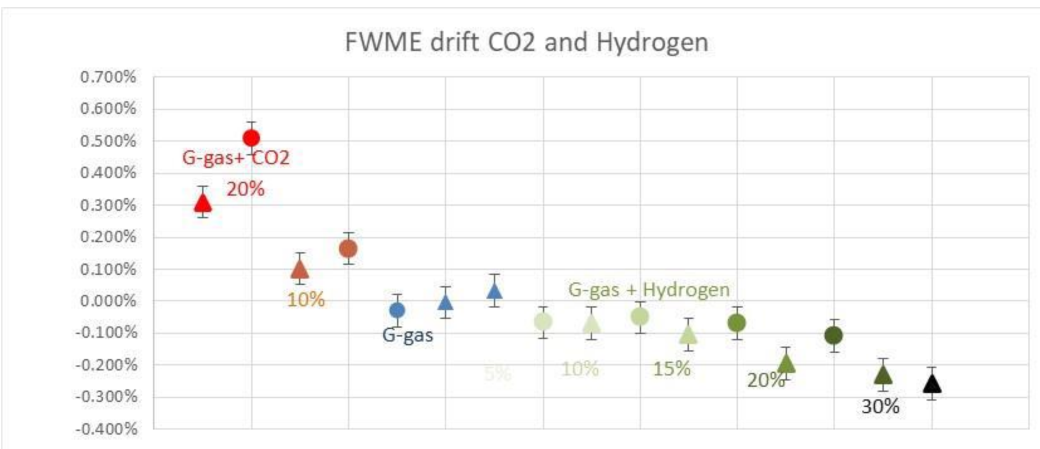

Figure 15: USM designed for natural gas (Example manufacturer B). The FWME results for various gases [18].

No systematic drift can be observed and further investigations are needed for the dependence on gas compositions.

It is worth to mention here, that ultrasonic gas meters for hydrogen blends up to 30 % are commercially available and certified according to the Measuring Instruments Directive 2014/32/EU (MID) for legal applications.

The authors do not have the knowledge of a common gas model for ultrasonic gas meters.

2.6 Coriolis mass flow meters

The Coriolis meter require a compensation for the operating pressure and the compressibility [12].

$$q_{g,CMF}^{c} = q_{g,CMF} \cdot f_p \cdot f_c \,,$$

where f_p is the pressure compensation factor and f_c the compressibility compensation factor, $q_{g,CMF}$ is the mass flow rate of the Coriolis mass flow meter [24].

$$f_p = \frac{1}{1 + a_p(p - p_c)}$$

with p_c is calibration pressure (2 bara) and a_p is a meter specific coefficient according to the data sheet, of the order -0.008 %/bar [24,25].

As example, the correction factor f_p is calculated for the operation pressure at 32 bara being f_p = 1.0024.

The compressibility correction is based on a theoretical model developed in [26] and requires the angular tube frequency ω, the tube radius r, and the speed of sound c, as an input. The compressibility compensation is then given by:

$$f_c = \frac{1}{1 + a_c \frac{1}{2}\left(\frac{\omega}{c} r\right)}$$

parameter a_c is an experience factor from the manufacturer and is typically close to 1.

A CMF300 [24] has been calibrated with water and natural gas at 9, 16 and 32 bar as shown in Figure 16.

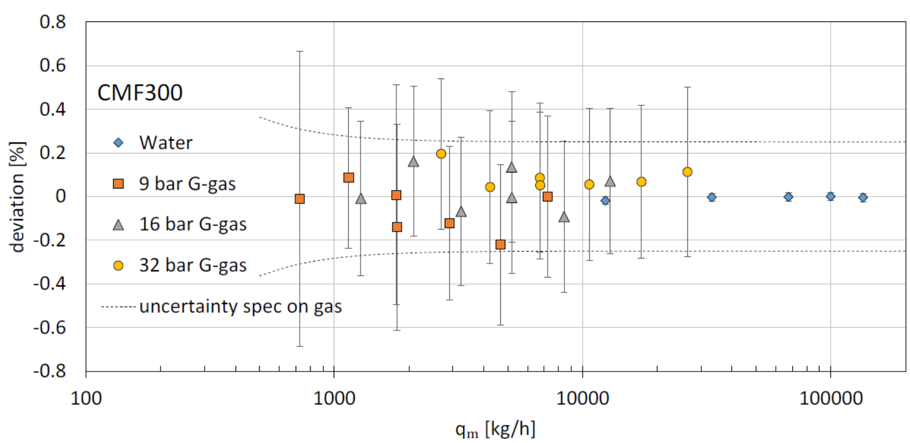

Figure 16: CMF300 calibration results for water and natural gas at 9, 16 and 32 bar. Error bars represent the measurement uncertainty including the CMC of the facility and the repeatability of the meter. The specified accuracy for gas is also indicated as dashed line [12].

It is important to note that the gas model used in Coriolis flow meters is often proprietary information of the manufacturer, as it is a crucial component of the meter's calibration and accuracy. Manufacturers typically perform extensive testing and calibration to ensure accurate measurement across a range of flow rates and fluid types. Therefore, the exact mathematical model and algorithms used in a specific Coriolis flow meter may not be publicly disclosed.
When selecting or working with Coriolis flow meters, it's essential to refer to the manufacturer's documentation and specifications for detailed information about the gas model and how it applies to the specific meter in use.

2.7 Thermal mass flow meter (TMFM)

The thermal mass flow meter senses flow by measuring the rate of heat transfer from a heated tube to the gas flowing inside the tube. The heater on the tube is provided by a constant input power and the temperature of the gas is measured on both sides of the heater. The measured difference in temperature is linearly dependent upon mass flow to first order according to [27]:

$$\dot{m} = \frac{Q_{CapWall-Gas}}{C_p(T)(T_{Gd} - T_{Gu})}$$

with $C_p(T)$ is the temperature dependent molar heat capacity, $Q_{CapWall\text{-}Gas}$ is the rate of heat transfer from the capillary wall to the gas, T_{Gd} is the gas temperature downstream of the heated capillary, T_{Gu} is the gas temperature upstream of the heated capillary and $\dot{m}$ is the molar flow.

Therefore, $Q_{CapWall\text{-}Gas}$ is also dependent on the thermal conductivity of the gas on the geometry of the sensor.

Nonlinearities may be introduced into the measurements by:

- The gas temperature is normally measured by measuring the temperature of the capillary wall, which should correspond to the gas stream temperature.
- $Q_{CapWall\text{-}Gas}$ might depend on the flow rate and not only on the gas properties.
- The heat capacity of the gas may be temperature dependent.
- Other heat loss mechanisms may introduce additional nonlinearities.

TMFM's are usually calibrated with dry air or nitrogen and corrected for other gases, but the correction factors are not well understood and depend on the design of the flow meter and on the properties of the gas such as heat capacity, heat transfer and density or molar mass.

These correction factors are instrument specific and communicated by the manufacturer [27].

2.7.1 Experimental vs recommended correction factors

Several experiments are reported, where the correction factors for gases were determined experimentally and compared to the recommended corrections factors from the manufacturer [27,28,29,30].

2.7.1.1 Calibrations with N_2, Ar, He, H_2, SF_6 and C_2F_6

Five TMFM's were calibrated with nitrogen, argon, helium, hydrogen, sulfur hexafluoride (SF_6) and hexafluoroethane (C_2F_6) and nitrogen was used as reference gas in order to determine experimentally the correction factors for the other gases as summarized in Table 1 [27]. Additionally, the correction factor predicted from the ratio of the specific heats at given temperatures of 50 °C and 100 °C are given in this table [31].

Table 1: Comparison of the measured gas correction factors (CF) for TMFM's with those predicted from the ratio of the gas specific heats at the given temperature (Cal CF) [27].

Gas	TMFM A (CF)	TMFM B (CF)	TMFM C (CF)	TMFM D (CF)	TMFM E (CF)	Cal CF (50 °C)	Cal CF (100 °C)
Helium	1.435	1.4400	1.4460	1.4740	1.4320	1.413	1.417
Argon	1.4260	1.4260	1.4260	1.4210	1.4180	1.395	1.397
SF_6	0.2750	0.2680	0.2720	0.2580	0.2810	0.285	0.257
C_2F_6	0.2667	0.2596	0.2629	0.2506	0.2513	0.262	0.238
H_2	1.1305	1.1075	1.1400	1.1600	1.1198	--	--

Depending on the gas and the correction factor recommended by the manufacturer, deviations from the recommended correction factor with respect to the experimentally determined correction factor are identified as large as 10 % or even larger for some single cases.

2.7.1.2 Calibrations with Air and Ar

Another group has investigated six TMFM's with air or argon as reference gas [29]. The TMFM's were configured for the one of the reference gas, which is then the process gas. Then the calibration is done with the other reference gas and the correction factor recommended by the manufacturer is applied and the deviation is determined. The deviations range from several percent up to tens of percent as shown in Figure 17 [29].

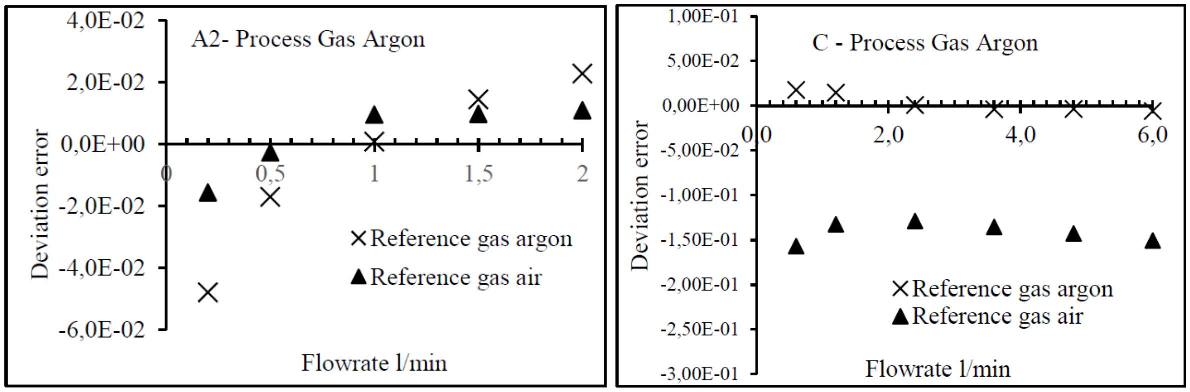

Figure 17: The deviation error of the TMFM A2 (left) and TMFM C (right) when calibrated with Air and Argon using Process Gas Argon [29]

2.7.1.3 Calibrations with Air, N_2, Ar, He and CO_2

Further investigations show that the theoretical correction factor, which depends on the specific heat and the density of the reference (ref) and process (proc) gas, can lead to large deviations in calibrations [28]. Here the correction factor k has been calculated according to

$$k = \frac{C_{p.ref} \cdot \rho_{n.ref}}{C_{p.proc} \cdot \rho_{n.proc}}$$

where C_p is the specific heat and ρ_n the density at normal conditions.

Also in this study the correction factors are slightly dependent on the flow rate and the deviations of the correction factors compared to the recommended correction factors by the manufacturer can be rather large from a metrological point of view (6%).

2.7.2 CFD simulation for correction factors for various gases

A Computational Fluid Dynamic solver has been used to develop a model for thermal flow meter based on capillary tubes with an inner diameter of 1 mm [30]. The molar mass flow rate is proportional to:

$$\dot{m} \propto \frac{\Delta T \; \dot{q} \; A}{C_p \; M}$$

where ΔT is the temperature difference, $\dot{q}$ is the supplied heat flux, A is the surface area of the heater, C_p is the specific heat and M is the molecular weight.

For a constant temperature difference, the correction factor is the ratio of the products of the specific heat C_p and the molecular weight M:

$$\frac{\dot{m}_1}{\dot{m}_2} = \frac{C_p\, M\big|_2}{C_p\, M\big|_1}$$

This allows to scale the characteristic curves obtained in Figure 18 (left) resulting in a master curve shown in Figure 18 (right).

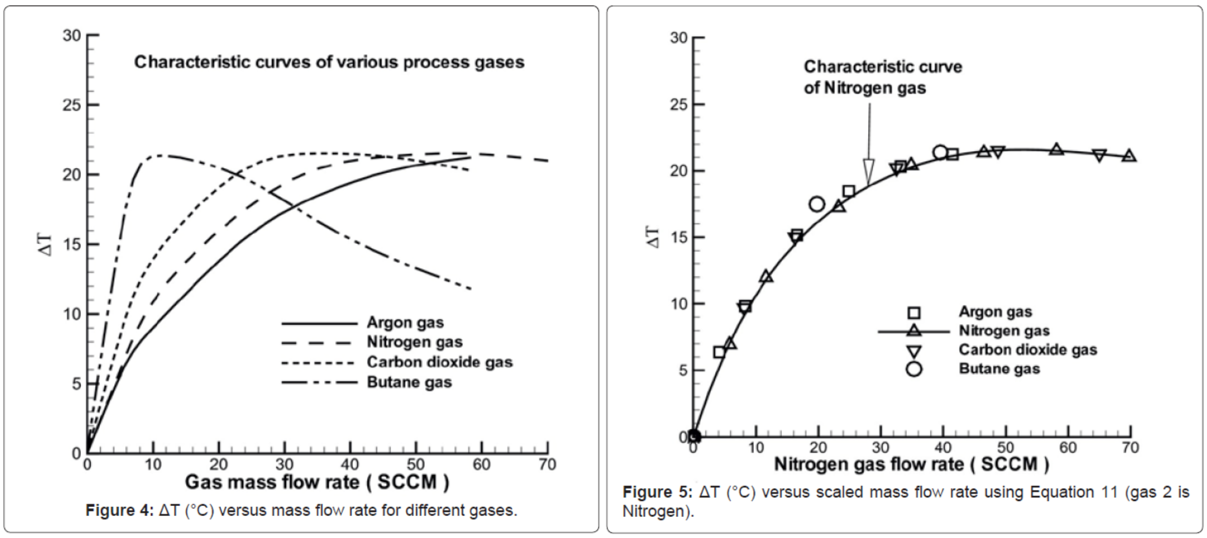

Figure 18: DT (°C) versus mass flow rate for different gases (left). DT (°C) versus scaled mass flow rate using the relation described above (right) [30].

Adding calculations for Ammonia, Methane, Helium, Ethane and Hydrogen reveals deviations of the scaled master curve of the order of several percent's (1 % – 8 %). Although, the prediction is accurately for many gases it shows considerable deviation for other gases. Therefore, a correction is proposed by applying another correction factor f [30]:

$\frac{\dot{m}_1}{\dot{m}_2} = \frac{C_p\, M|_2}{C_p\, M|_1} * f$ with the correction factor $f = \frac{1}{(1+\varepsilon)}$

ε is a parameter modeled as a modified Gaussian radial basis function with γ as independent variable. The use of γ accounts for the compressibility effects of the gas, if any. The proposed form of the equation is:

$100\varepsilon = A + B\left(e^{-Cr^2}\right) + D\left(e^{-Cr^2}\right)^2$ where $r = (\gamma - 1.28)$

A regression analysis of the data from nine different gases yields the parameters A, B, C and D. Applying these parameters for the calculation of ε and the correction factors f and $\dot{m}_1/\dot{m}_2$, results in deviations smaller than 2 % for all the cases considered in this study.

Moreover, calculations show a minimal effect of pressure on the mass flow meter for a pressure drop from 1 bar to 10 mbar leading to a change in $\Delta T < 1$ %, which is rather small.

3 Discussion and conclusion

As mentioned in the previous chapters, different gas flow meter technologies have been tested with various gases, but not all of them have been tested with hydrogen. For some gas meter technologies predictive models for hydrogen are given, but the extensive experimental validation of these models is still missing.

- The critical flow venturi nozzles have been tested with various gases, where air, nitrogen and hydrogen showed similar behavior for the relative deviations in the same Reynolds number range. An extrapolation model has been presented, but the experimental validation has only been performed with natural gas. Tests with hydrogen are planned in the project MetHyInfra.
- Turbine meters have been investigated with blends up to 30 % of hydrogen in natural gas. A predictive model for meter deviation with hydrogen exists, but is has not yet been validated with hydrogen measurements.
- For the rotary meter a predictive model also exists, but measurements have only been performed with natural gas so far. Measurements with HENG have been performed in the framework of the project NEWGASMET [32]. Measurements with hydrogen are still missing.
- Differential pressure meters have only been tested with natural gas. Measurements with hydrogen are still missing.
- Ultrasonic meters have been investigated with blends up to 30 % of hydrogen in natural gas. Measurements with hydrogen are still missing.
- Coriolis flow meters have been investigated with natural gas. Measurements with hydrogen are still missing.
- Thermal gas flow meters have been tested with various gases including hydrogen, but the predictive models do not match the experimental results with the necessary accuracy.

Extensive experimental validation of the existing models for the different gas meter technologies are still missing. Therefore, the assessment whether models for air or natural gas can correctly model hydrogen flow is not possible at this stage due to lack of experimental data. A wide range of datasets is needed to estimate the limitations and expected uncertainties of the models.

It is expected that with the upcoming projects related to hydrogen this issue will be covered in the near future.

4 References

[1] M. Ishibashi, M. Takamoto. Theoretical discharge coefficient of a critical circular-arc nozzle with laminar boundary layer and its verification by measurements using super-accurate nozzles. Flow Meas. and Instr. 11(4), 2000,305-313.

[2] ISO 9300: Measurement of gas flow by means of critical flow Venturi nozzles, 2022.

[3] B. Mickan, Discharge coefficients of CFVN predicted for high Reynolds numbers based on low-Re-calibration, Flow Meas. Instrum. 78 (2021).

[4] J.R. Kliegel, J.N. Levine, Transonic flow in small throat radius of curvature nozzles, AIAA J. 7 (1969) 1375 – 1378.

[5] B.S. Stratford, The calculation of the discharge coefficient of profiled choked nozzles and the optimum profile for absolute air flow measurement. J. Royal Aeronautical Soc. 68 (1964) 237 – 245.

[6] D. Geropp. Laminare Grenzschichten in ebenen und rotationssymmetrischen Lavalduesen. Deutsche Luft- und Raumfahrt. Forschungsbericht 71-90, 1971.

[7] D. Geropp. Laminare Grenzschichten in Überschalldüsen. Deutsche Luft- und Raumfahrt. Forschungsbericht 01 TM 8603-AK/PA 1, 1987.

[8] G. Bobovnik, B. Mickan et al. Investigation of the discharge coefficient in the laminar boundary layer regime of critical flow Venturi nozzles calibrated with different gases including hydrogen. Measurement 217 (2023) 113134.

[9] B. Mickan, J.-P. Vallet, C. Li, J. Wright. Extended data analysis of bilateral comparisons with air and natural gas up to 5 MPa. Flomeko 2016, Sydney, Australia, September 26-29, 2016.

[10] B. Mickan, Discharge coefficients of CFVN predicted for high Reynolds numbers based on low-Re-calibration, Flow Meas. Instrum. 78 (2021).

[11] B. Mickan, Discharge coefficients of CFVN predicted for high Reynolds numbers based on low-Re-calibration, Flomeko conference, 2019, Lisbon, proceeding paper. https://www.imeko.info/publications/tc9-2019/IMEKO-TC9-2019-038.pdf

[12] J. van der Grinten, B. Mickan, H. Riezebos and D. van Putten. Gas flow traceability for non-conventional and renewable gases. 39th International North Sea Flow Measurement Workshop, 26 – 29 October 2021.

[13] https://www.methyinfra.ptb.de/the-project/

[14] J. van der Grinten, A. Gunnarsson, M. van der Beek and B. Mickan (2019): *An intercomparison between primary high-pressure gas flow standards with sub-permille uncertainties*, 37th International North Sea Flow Measurement Workshop, Tønsberg, Norway, 22 - 24 October 2019, Reprinted in Cal Lab: The International Journal of Metrology, vol 27(4), 2020, pp 28-35.

[15] H.-B. Böckler. Messrichtigkeit von mechanischen Gasmessgeräten bei Verwendung von unterschiedlichen Gasbeschaffenheiten, Dissertation, Universität Duisburg-Essen, 2019, ISBN 978-3-95606-493-7

[16] B. Mickan, H.-B. Böckler, D. Schumann and J. van der Grinten. Transferability of calibration results obtained with conventional gases for application with hydrogen, Flomeko conference, 2022, Chongqing, China, proceeding paper. DOI: 10.21014/tc9-2022.159, https://www.imeko.org/publications/tc9-2022/IMEKO-TC9-2019-159.pdf

[17] EuReGa (2018): EuReGa Communique No. 2 Harmonized Reference Value 2018, Euramet F1301. https://tinyurl.com/yyzhb58l

[18] D. van Putten, H. Riezebos, M. Al Saleem. *Assessment of renewable gases influence on gas flow meters*. 39th International North Sea Flow Measurement Workshop, 26 – 29 October 2021, Presentation of Paper 12*, results on performance of turbine and ultrasonic flow meters up to 30% Hydrogen and 20% CO2*.

[19] ISO 17089-1:2019. Measurement of fluid flow in closed conduits – Ultrasonic meters for gas – Part 1: Meters for custody transfer and allocation measurement.

[20] ISO 5167-2: *Measurement of fluid flow by means of pressure differential devices inserted in circular-cross section conduits running full — Part 2: Orifice plates*, 2003

[21] E. Starke, F. Ullmann, J. Ruschke. Ultraschall Mengenmessung von Wasserstoff und wasserstoffhaltigen Gasgemischen – Erfahrungen, Herausforderungen und Ausblick. 11. Workshop Gasmengenmessung – Gasanlagen – Gastechnik 2022, 30 – 31 March 2022, KCE-Akademie in Rheine, Germany

[22] EMPIR 20IND10 Decarb, Metrology for decarbonizing the gas grid.

[23] EMPIR 21GRD05 Met4H2, Metrology for the hydrogen supply chain.

[24] Emerson: *Micro Motion™ ELITE™ Coriolis Flow and Density Meters*, Product Data Sheet PS-00374, Rev AK, January 2020

[25] Endress+Hauser: Proline Promass F 300, Coriolis Flow Meter, Technical Information TI01221D/06/DE/10.22-00 71551573, 2022-08-01.

[26] J. Hemp and J. Kutin: *Theory of errors in Coriolis flowmeter readings due to compressibility of the fluid being metered*, Flow Measurement and Instrumentation 17 (2006) 359–369.

[27] S.A. Tison. A critical evaluation of thermal mass flow meters. J. Vac. Sci. Technol. A 14(4), pp. 2582-2591, Jul/Aug 1996.

[28] PN Unnikrishnan, KG Sivaprakash, J Chandapillai. Conversion factors for Thermal Mass flow meters for different operating mediums: An Experimental study. Conference flotek.g 2017, August 28-30, 2017, FCRI, Palakkad, Kerala, India.

[29] O. ABBAS, F. Mouchel. The influence of Gas Type on a Thermal Mass Flowmeter Calibration Results. 19th International Congress of Metrology, 21002, 2019.

[30] Sashi Kumar GN, Mahendra AK, Gouthaman G. Understanding the Compatibility of Thermal Mass Flow Meter with Various Process Gases. J Chem Eng Process Technol, S1:002, 2011.

[31] ISO 14511, Measurement of fluid flow in closed conduits – Thermal mass flowmeters, second edition – ISO (2019).

[32] https://newgasmet.eu/the-project